



Mitigate self-compensation with high crystal symmetry: A first-principles study of formation and activation of impurities in GaN

Yi-Chia Tsai, Can Bayram*

Department of Electrical and Computer Engineering, University of Illinois at Urbana-Champaign, Urbana, IL 61801, USA
 Holonyak Micro and Nanotechnology Laboratory, University of Illinois at Urbana-Champaign, Urbana, IL 61801, USA

ARTICLE INFO

Keywords:

Activation energy
 First-principles calculations
 Formation energy
 p-type doping
 Vibrational entropy
 Zincblende GaN

ABSTRACT

Formation and activation energies of common impurities: silicon (Si), germanium (Ge), carbon (C), beryllium (Be), and magnesium (Mg) in wurtzite (wz-) and zincblende (zb-) GaN are investigated by first-principles calculations. Si and Ge are excellent donors with low activation energies (<30 meV). The acceptor activation energies of C and Be in wz-GaN (and zb-GaN) are found to be 590 and 205 meV (and 490 and 134 meV), respectively. Neither C nor Be is a qualified acceptor in general as the former has a large activation energy (>300 meV) and the latter has a strong self-compensation effect (the formation energy of Be_i compensating donor is negative). Be_i is energetically abundant in zb-GaN because it has a 0.66 eV lower formation energy than wz-GaN. This is attributed to the coherence of the symmetry between the s-orbitals and the interstitial site. The acceptor activation energy of Mg in zb-GaN is found to be 153 meV, which is smaller than its value in wz-GaN, 226 meV. Vibrational analysis suggests that Mg_i compensating donor is less favorable to form in zb- than wz-GaN, since the higher symmetry of the interstitial site in zb-GaN renders a much smaller vibrational entropy. Contrarily, the differences are insignificant for the impurities residing on Ga sites due to the same tetrahedral symmetry. The results evidence the importance of self-compensation effects, which can be mitigated by the higher crystal symmetry of zb-GaN.

1. Introduction

Gallium nitride (GaN) and its alloys are the mainstream semiconductors used in high-electron-mobility transistors (HEMTs) and light-emitting diodes (LEDs). N- and p-type doping is essential to the realization of the wide-range applications. Achieving electron and hole concentrations beyond 10^{19} cm^{-3} in GaN is alluring as it would enhance carrier injection.[1,2] The n- and p-type dopability of GaN is determined by the formation, activation, and self-compensation of dopants. Common donors-silicon (Si) and germanium(Ge)-are measured to have small activation energies of <30 meV;[3,4] yet, large activation energies of 890, 200, and 225 meV are measured in carbon (C)-, beryllium (Be)-, and magnesium (Mg)-doped wurtzite (wz-) GaN, respectively.[5-7] Until recently, the amphoteric natures of Be and Mg dopants are discussed in wz-GaN.[8-10] The poor hole injection in GaN-based devices is a hitherto challenge.[11-13]

An ideal solution should equip the same n-type dopability, a lower acceptor activation energy, and a weaker self-compensation effect. Zincblende (zb-) GaN featuring lighter electron and hole effective

masses is a potential alternative to have shallower donor and acceptor levels,[14-18] which have been preliminarily predicted by the effective-mass theory.[19,20] However, the acceptor levels deviate from measurements.[16] This is because the effective doping concentration is prone to the presence of other doping configurations and charge states. Neglecting the impacts has a proclivity to overestimate the activation energy. The impacts of different doping configurations and charge states on carrier concentrations remain vague, as are the self-compensation effects. Bridging the gap necessitates first-principles calculations.

In this work, the formation energies, activation energies, and self-compensation effects of wz- and zb-GaN with Si, Ge, C, Be, and Mg incorporations are first examined. A detailed comparative study between Mg-doped wz- and zb-GaN is carried out by considering vibrational contributions. Eventually, the hole concentrations are estimated to indicate that higher hole concentrations are achievable with zb-GaN.

2. Methodologies

96-atom wz-GaN and 64-atom zb-GaN supercells are constructed.

* Corresponding author at: Department of Electrical and Computer Engineering, University of Illinois at Urbana-Champaign, Urbana, IL 61801 USA.
 E-mail address: cbayram@illinois.edu (C. Bayram).

The atomic structures with an impurity incorporated on a tetrahedral interstitial site, an octahedral interstitial site, a Ga site, and an N site, are illustrated in Fig. 1. The defective geometries are relaxed by the Heyd-Scuseria-Ernzerhof functional implemented in Vienna *ab initio* simulation package[21] with the optimal Hartree-Fock mixing of 0.302.[15] The first-principles calculations are performed at 0 K, where all electrons fill up valence bands. A cut-off kinetic energy of 500 eV is employed for projector-augmented wave pseudopotentials. The Brillouin zones of the wz- and zb-supercells are sampled within the Monkhorst-Pack scheme using $2 \times 1 \times 1$ and $2 \times 2 \times 2$ k-points, respectively. The Γ point, where the interaction between the impurity and its periodic images reaches a maximum, is purposely excluded. [22]

The formation energy of an impurity X in a charge state q at a given temperature T is defined as follows:

$$E^f[X^q; T] = E_{tot}[X^q] - E_{tot}[GaN] - \sum_i n_i \mu_i + q(E_v + E_F + \Delta V) + E_{corr}^q + \Delta E[X^q; T], \quad (1)$$

where $E_{tot}[X^q]$ and $E_{tot}[GaN]$ are the free energies of the defective and pristine supercells, respectively. n_i is the number of the atom i added ($n_i > 0$) or removed ($n_i < 0$) with the chemical potential of μ_i listing in Table 1. E_F is the Fermi level referenced to the valence band maximum E_v (VBM), where ΔV is the band alignment term between the defective and pristine GaN. E_{corr}^q is the correction energy for the nonphysical Coulomb interaction between the impurity and its periodic images. The static dielectric constants of 10.63 and 9.82 obtained from the Lyddane-Sachs-Teller relation are applied for wz- and zb-GaN, respectively. $\Delta E[X^q; T]$ represents the vibrational corrections, expressed by:

$$\Delta E[X^q; T] = F_{vib}[X^q; T] - F_{vib}[GaN; T] - \sum_i n_i \mu_i^{vib}(T), \quad (2)$$

where $F_{vib}[X^q; T]$ and $F_{vib}[GaN; T]$ are the vibrational free energies of the defective and pristine supercells, respectively. $\mu_i^{vib}(T)$ is the vibrational free energy of the atom i . The chemical potential of N_2 is related to partial pressure and rotational contributions using standard thermodynamic expressions.[23] F_{vib} and μ_i^{vib} are determined based on the quasi-harmonic approximation implemented in *Phonopy*,[24] where the force constants are calculated by the Perdew-Burke-Ernzerhof functional.

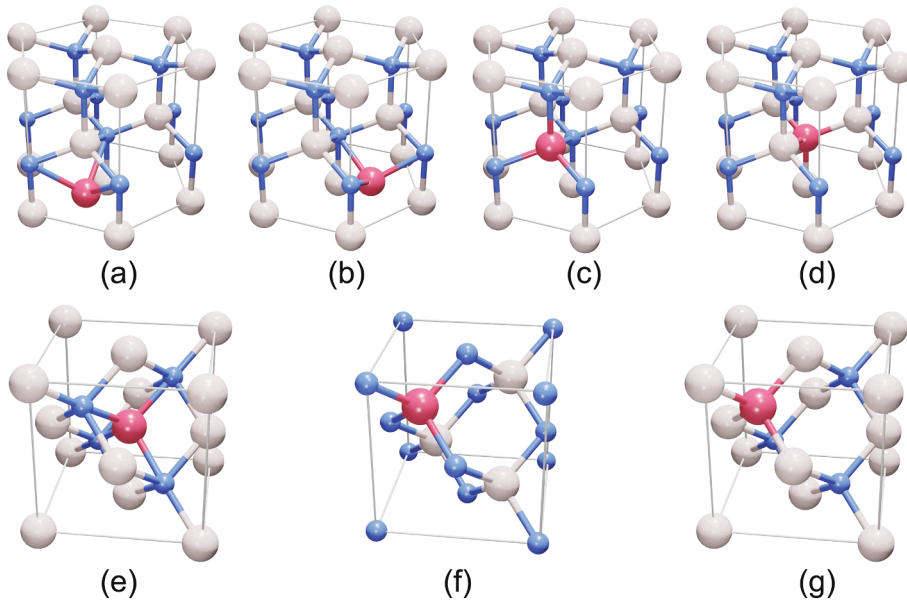


Fig. 1. Atomic structures with an impurity, indicated by a red sphere, residing on (a) a tetrahedral interstitial site, (b) an octahedral interstitial site, (c) a Ga site, and (d) an N site in wz-GaN and (e) a tetrahedral interstitial site, (f) a Ga site, and (g) an N site in zb-GaN. White and blue spheres represent Ga and N atoms, respectively.

Table 1

Chemical potential of elemental species in pure bulk (or gas) phase, Ga-rich condition, and N-rich condition, where the enthalpy of formation (ΔH_f) of solubility-limiting compounds is determined and compared with experiments. All values are in unit of eV/f.u.

Species	Bulk/Gas	Ga-rich	N-rich	Compounds	ΔH_f	ΔH_f^{exp}
Ga	-3.417	-3.417	-4.408	GaN	-1.094	-1.136
N	-10.82 ^a	-11.81	-10.82	-	-	-
Be	-3.779	-5.003	-5.663	Be ₃ N ₂	-5.859	-6.097
C	-10.88 ^b	-10.88	-10.88	C ₃ N ₄	3.054	-
Mg	-1.524	-2.171	-2.831	Mg ₃ N ₂	-4.129	-4.778
Si	-6.480	-7.948	-9.269	Si ₃ N ₄	-8.780	-8.592
Ge	-5.476	-5.476 ^c	-5.521	Ge ₃ N ₄	-0.547	-0.653

^a Chemical potential of N_2 is related to partial pressure (101.325 kPa), temperature (298.15 K), and rotational contribution via standard thermodynamic expressions.[23]

^b Chemical potential of C is given by the energy of graphite.

^c Chemical potential of Ge in Ga-rich conditions is given by the energy of the elemental bulk phase.

3. Results and discussion

Fig. 2 shows the formation energies of various doping configurations in (a) wz-GaN and (b) zb-GaN as a function of Fermi level under Ga-rich conditions, where the vibrational contributions are ignored. For n-type doping, Si and Ge donors are stable on Ga sites with low activation energies (<30 meV). Si and Ge impurities residing on N sites and interstitial sites have large formation energies (>5 eV) due to strong lattice distortion. The formation energies of Si_{Ga} and Ge_{Ga} in zb-GaN are close to the wz-counterparts at the VBM, however, the values are 0.2 eV smaller in zb- than wz-GaN at the conduction band minimum (CBM). This is because less energy is needed to remove an electron from the CBM. The evidence agrees with the conduction band offset of wz-/zb-GaN interface measured from the experiment.[25] For p-type doping, C_N is stable in +1, 0, and -1 charge states, where the (+/0) and (0/-) thermodynamic transition levels locate at 387 and 591 meV in wz-GaN and 99 and 492 meV in zb-GaN, respectively. The acceptor activation energy, i.e. the (0/-) level, falls within a range between 230 and 890 meV measured from experiments.[5] A broad prediction of 200–900 meV was also reported.[22,26] The variation may have originated from the strong interaction between C_{Ga} and C_N under p-type conditions. In

fact, the evidence of blue luminescence peaking at 2.86 eV, which is in close agreement with 2.89 eV extracted from Fig. 2, was attributed to the migration from a C_{Ga} donor to a C_N acceptor. [27] The blue luminescence is predicted to peak at 2.70 eV for C in zb-GaN. However, the high formation (>3 eV) and activation energies (>300 meV) render C as a poor acceptor for both wz- and zb-GaN. Be_{Ga} and Mg_{Ga} acceptors are stable in 0 and -1 with the activation energies of 205 and 226 meV in wz-GaN and 134 and 153 meV in zb-GaN, respectively. The activation energies of Be and Mg in wz-GaN agree with the measurements of 200 and 225 meV, [7,6] respectively. On the other hand, the activation energies of Be and Mg in zb-GaN are in accordance with 117–133 and 123–140 meV, respectively, as predicted by the effective-mass theory. [20] The formation energy of Mg_{Ga} is 0.5 eV smaller than Be_{Ga} because the atomic size of Mg is comparable with Ga, i.e. Mg impurity imposes less lattice distortion. However, Be and Mg energetically favor the interstitial site in p-type conditions. Notably, it has been found that impurities residing on the octahedral interstitial site are more stable than those on the tetrahedral interstitial site. Thus, the discussion on interstitial impurities in wz-GaN is based on the octahedral interstitial site. Unfortunately, Be_i and Mg_i are double donors, which render strong self-compensation effects and their formation energies are negative near the VBM. In wz-GaN, the formation energy of Be_i is 0.5 eV lower than Mg_i , meaning that Be suffers from a stronger self-compensation effect than Mg. The self-compensation effect of Be is adversely inexorable in zb-GaN since the formation energy of Be_i is 0.66 eV lower in zb- than wz-GaN. In general, it is found that the formation energies of C_i , Si_i , and Ge_i are lower in wz- than zb-GaN, but the formation energies of Be_i and Mg_i behave oppositely. This is because the impurities on the interstitial site are stable in +2 charge state, i.e. losing two electrons. The hypothesis is that the group-IV elements, such as C, Si, and Ge, bond with the neighbors by donating two p -orbital electrons. The p -orbitals are directional, hence maintaining the centrosymmetric nature of the interstitial site in zb-GaN necessitates more energy. Contrarily, the outermost core of the group-II elements, such as Be and Mg, are two s -orbital electrons, which satisfy the centrosymmetric nature inherently. The formation energy of Mg_i in zb-GaN, however, is close to that of wz-GaN due to the large atomic size of Mg. Consequently, Mg-doped zb-GaN has a smaller activation energy relative to Mg-doped wz-GaN without suffering from a stronger self-compensation effect, which is not the case found in Be. Given the complex interplay among Mg_{Ga} , Mg_{Ga}^0 , and Mg_i^{+2} , it is critical to quantify their impacts on hole concentrations.

Fig. 3(a) calculates the vibrational corrections of Mg_i and Mg_{Ga} in wz- and zb-GaN as a function of temperature under Ga-rich conditions. The vibrational corrections decrease for the elevated temperature due to the positivity of vibrational entropy (S) determined correspondingly in

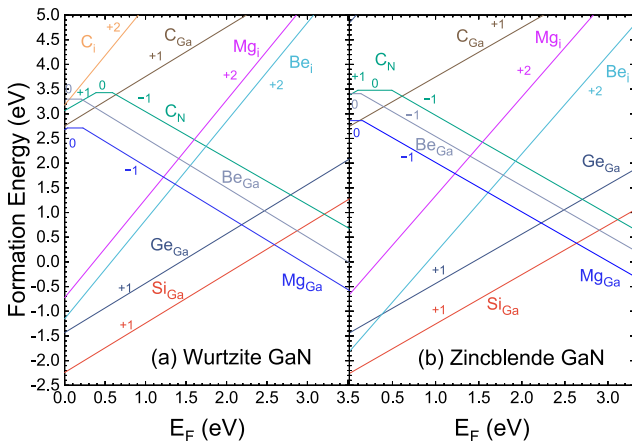


Fig. 2. Formation energies of various doping configurations in (a) wz- and (b) zb-GaN as a function of Fermi level under Ga-rich conditions.

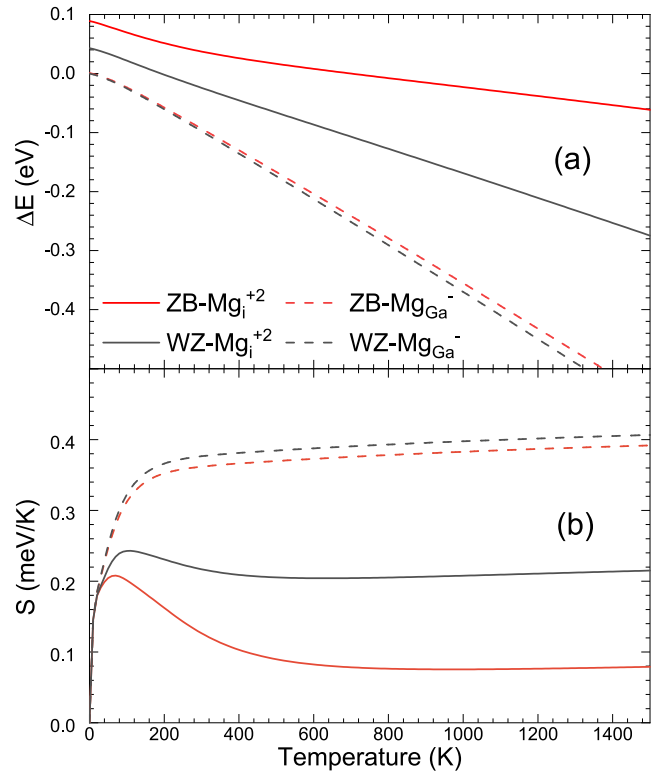


Fig. 3. (a) Vibrational corrections and (b) vibrational entropy of Mg_i double donor and Mg_{Ga} acceptor in wz- (black) and zb-GaN (red) as a function of temperature.

Fig. 3(b). Given the uneven numbers of species between the defective and pristine GaN, the vibrational entropy used for comparisons is determined by the first derivative of Eq. 2. It implies that the vibrational entropy used for comparisons is a linear combination of the vibrational entropy of each factor formulated in Eq. 2. In general, the vibrational entropy of the defective GaN is larger than pristine GaN due to the symmetry breaking, hence the difference in vibrational free energies between the defective and pristine GaN increases with respect to the increased temperature. This explains the declination of vibrational corrections. Interestingly, the vibrational correction of Mg_i is 186 meV larger in zb- than wz-GaN at 1300 K, indicating that Mg_i is much energetically abundant in wz-GaN. This fact can be ascribed to the symmetry of the interstitial site in zb-GaN, which leads to a substantially smaller vibrational entropy as opposed to the wz-counterpart as shown in Fig. 3(b). The bonding nature between Mg_{Ga} and 4 nitrogen neighbors satisfies sp^3 -hybridization in both wz- and zb-GaN due to the same tetrahedral symmetry. As a result, the vibrational correction of Mg_{Ga} in zb-GaN is merely 19 meV larger than that of wz-GaN at 1300 K. Indeed, the small differences of 17 and 21 meV are found for Si_{Ga} and Ge_{Ga} as well, which reinforce the hypothesis.

The concentrations of Mg_{Ga} and Mg_i are determined by the respective Boltzmann factors for a given Mg concentration and temperature. The Fermi level is solved self-consistently by satisfying the charge neutrality. The electron and hole concentrations are formulated in the Boltzmann approximation where the electron and hole effective masses of 0.20 and 1.50 (and 0.13 and 1.40) m_0 are applied to wz-GaN (and zb-GaN), respectively. Fig. 4(a) calculates the hole concentrations and $[Mg_i]/[Mg_{Ga}]$ as a function of Mg concentration at 1300 K. The hole concentrations increase linearly when $[Mg] < 10^{16} \text{ cm}^{-3}$, because all the acceptors are ionized at 1300 K. However, the concentration of compensating donor surges when the Fermi level is close to the position where the formation energies of Mg_i and Mg_{Ga} are identical. Ultimately, the self-compensation effect causes the Fermi-level pinning and the

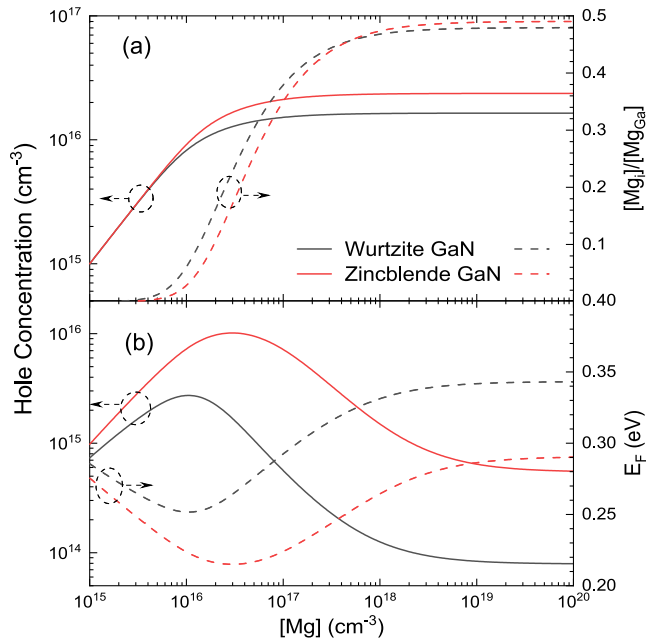


Fig. 4. (a) Hole concentrations and $[Mg_i]/[Mg_{Ga}]$ as a function of Mg concentration at the growth temperature of 1300 K. (b) Hole concentrations and Fermi levels as a function of Mg concentration at 300 K.

saturation of hole concentrations. Under this scenario, the maximum hole concentration is 44.3% higher in zb- than wz-GaN. The improvement is a direct reflection on the larger formation energy of Mg_i relative to the wz-case. After a rapid thermal quench to 300 K, the equilibrium impurity concentrations are preserved. At 300 K, the compensating donor is fully ionized. Yet, the ionized acceptor concentration is determined by the activation energy (E_A), expressed by

$$[Mg_{Ga}^-] = \frac{[Mg_{Ga}]}{1 + \beta e^{-\frac{E_F - E_A}{k_B T}}} \quad (3)$$

where $\beta = 4$ is the valence-band degeneracy. Fig. 4(b) estimates the hole concentrations and the Fermi levels as a function of Mg concentration at 300 K. When juxtaposed to Fig. 4(a), the maximum hole concentration is 3.7 times larger in zb- than wz-GaN due to the smaller activation energy of Mg-doped zb-GaN. However, once the maximum hole concentration is reached, the surplus Mg dopants favor the interstitial site and eventually drop the hole concentrations. In this state, the hole concentration of Mg-doped zb-GaN is more than an order higher than Mg-doped wz-GaN. The lowest Fermi levels in Mg-doped wz- and zb-GaN are 252 and 215 meV, which coincide with the measured activation energies, respectively. Indeed, if the self-compensation effect is neglected, the Fermi level of degenerately-doped GaN positions close to its activation energy. It is practicable that the extraction of activation energies does not have the self-compensation effect considered. It can be evidenced by the fact that the Fermi level still pins at 215 meV even though the much smaller activation energy of 153 meV is procured in Mg-doped zb-GaN. The results suggest the significance of self-compensation effects that must be accounted for in experimental extractions.

It is worth noting that the qualitative analysis is carried out for several reasons. First of all, calculating absolute hole concentration necessitates the consideration of nitrogen vacancy, which not only compensates acceptors but competes with Mg_i . Consequently, the proliferation of Mg_i occurs at a much higher Mg concentration of 10^{19} cm^{-3} rather than 10^{17-3} observed in our case. Second, the self-consistent bulk calculations would bring the Fermi level closer to VBM promoting the self-compensation effect. Third, the surface band bending resulting from Mg incorporation, on the contrary, would push the Fermi level away

from VBM. Howbeit, according to the nonequilibrium model, [8] which enables compensating donors selectively, the neglected effects shift the threshold concentration effectively. Therefore, it is expected that the qualitative behavior is less dependent on the neglected effects.

4. Conclusion

The formation, activation, and self-compensation of donors (Si and Ge) and acceptors (C, Be, and Mg) in wz- and zb-GaN are investigated by first-principles calculations. For n-type doping, Si and Ge are shallow donors in both wz- and zb-GaN with low activation energies (<30 meV). For p-type doping, the activation energies of C and Be in zb-GaN are 490 and 134 meV compared to 590 and 205 meV found in wz-GaN, respectively. Neither C nor Be is an excellent acceptor in both wz- and zb-GaN as the former suffers from a large activation energy and the latter is subject to a strong self-compensation effect. Be_i is energetically much abundant in zb- than wz-GaN because of the small atomic size and the coherence of the symmetry between the s-orbitals and the interstitial site. The activation energy of 153 meV is procured for Mg-doped zb-GaN, which is smaller than 226 meV in Mg-doped wz-GaN. Through the vibrational analysis, Mg_i formation is less favorable in zb- than wz-GaN because of the large vibrational entropy difference, which is inconsequential for the impurities residing on Ga sites due to the same tetrahedral symmetry. The importance of self-compensation during the extraction of activation energies has been evidenced. zb-GaN featuring a higher crystal symmetry has the potential to mitigate the self-compensation and realize a fourfold higher hole concentration.

Data availability

The raw/processed data required to reproduce these findings cannot be shared at this time due to technical or time limitations.

Declaration of Competing Interest

The authors declare that they have no known competing financial interests or personal relationships that could have appeared to influence the work reported in this paper.

Acknowledgements

This work is supported by the National Science Foundation Faculty Early Career Development (CAREER) Program under award number NSF-ECCS-16-52871. The authors acknowledge the computational resources allocated by the Extreme Science and Engineering Discovery Environment (XSEDE) with No. TG-DMR180075.

References

- [1] H. Morkoç, Handbook of Nitride Semiconductors and Devices, Vol. 1, Wiley, 2008. doi:10.1002/9783527628438.
- [2] J.N. Baker, P.C. Bowes, J.S. Harris, R. Collazo, Z. Sitar, D.L. Irving, Complexes and compensation in degenerately donor doped GaN, Appl. Phys. Lett. 117 (10) (2020), 102109, <https://doi.org/10.1063/5.0013988>.
- [3] N. Young, R. Farrell, M. Iza, S. Nakamura, S. DenBaars, C. Weisbuch, J. Speck, Germanium doping of GaN by metalorganic chemical vapor deposition for polarization screening applications, J. Cryst. Growth 455 (2016) 105–110, <https://doi.org/10.1016/j.jcrysgro.2016.09.074>.
- [4] K. Ueno, T. Fudetani, Y. Arakawa, A. Kobayashi, J. Ohta, H. Fujioka, Electron transport properties of degenerate n-type GaN prepared by pulsed sputtering, APL Mater. 5 (12) (2017), 126102, <https://doi.org/10.1063/1.5008913>.
- [5] C.H. Seager, A.F. Wright, J. Yu, W. Götz, Role of carbon in GaN, J. Appl. Phys. 92 (11) (2002) 6553–6560, <https://doi.org/10.1063/1.1518794>.
- [6] T. Cheng, S. Hooper, L. Jenkins, C. Foxon, D. Lacklison, J. Dewsnip, J. Orton, Optical properties of doped GaN grown by a modified molecular beam epitaxial (MBE) process on GaAs substrates, J. Cryst. Growth 166 (1–4) (1996) 597–600, [https://doi.org/10.1016/0022-0248\(96\)00057-7](https://doi.org/10.1016/0022-0248(96)00057-7).
- [7] B. Monemar, P.P. Paskov, G. Pozina, C. Hemmingsson, J.P. Bergman, S. Khromov, V.N. Izyumskaya, V. Avrutin, X. Li, H. Morkoç, H. Amano, M. Iwaya, I. Akasaki, Properties of the main Mg-related acceptors in GaN from optical and structural

- studies, *J. Appl. Phys.* 115 (5) (2014), 053507, <https://doi.org/10.1063/1.4862928>.
- [8] G. Miceli, A. Pasquarello, Self-compensation due to point defects in Mg-doped GaN, *Phys. Rev. B* 93 (16) (2016), 165207, <https://doi.org/10.1103/PhysRevB.93.165207>.
- [9] F. Tuomisto, V. Prozhveeva, I. Makkonen, T.H. Myers, M. Bockowski, H. Teisseyre, Amphoteric Be in GaN: Experimental Evidence for Switching between Substitutional and Interstitial Lattice Sites, *Phys. Rev. Lett.* 119 (19) (2017), 196404, <https://doi.org/10.1103/PhysRevLett.119.196404>.
- [10] G. Miceli, A. Pasquarello, Migration of Mg and other interstitial metal dopants in GaN, *Phys. Status Solidi – Rapid Res. Lett.* 11 (7) (2017) 1700081, <https://doi.org/10.1002/pssr.201700081>.
- [11] U. Kaufmann, P. Schlotter, H. Obloh, K. Köhler, M. Maier, Hole conductivity and compensation in epitaxial GaN: Mg layers, *Phys. Rev. B* 62 (16) (2000) 10867–10872, <https://doi.org/10.1103/PhysRevB.62.10867>.
- [12] C.G. Van de Walle, S. Limpijumnong, J. Neugebauer, First-principles studies of beryllium doping of GaN, *Phys. Rev. B* 63 (24) (2001), 245205, <https://doi.org/10.1103/PhysRevB.63.245205>.
- [13] C.A. Hernández-Gutiérrez, Y.L. Casallas-Moreno, V.-T. Rangel-Kuoppa, D. Cardona, Y. Hu, Y. Kudriatsev, M.A. Zambrano-Serrano, S. Gallardo-Hernandez, M. Lopez-Lopez, Study of the heavily p-type doping of cubic GaN with Mg, *Sci. Rep.* 10 (1) (2020) 16858, <https://doi.org/10.1038/s41598-020-73872-w>.
- [14] R. Liu, R. Schaller, C.Q. Chen, C. Bayram, High Internal Quantum Efficiency Ultraviolet Emission from Phase-Transition Cubic GaN Integrated on Nanopatterned Si(100), *ACS Photonics* 5 (3) (2018) 955–963, <https://doi.org/10.1021/acsp Photonics.7b01231>.
- [15] Y.-C. Tsai, C. Bayram, Band Alignments of Ternary Wurtzite and Zincblende III-Nitrides Investigated by Hybrid Density Functional Theory, *ACS Omega* 5 (8) (2020) 3917–3923, <https://doi.org/10.1021/acsomega.9b03353>.
- [16] D.J. As, T. Simonsmeier, B. Schöttker, T. Frey, D. Schikora, W. Kriegseis, W. Burkhardt, B.K. Meyer, Incorporation and optical properties of magnesium in cubic GaN epilayers grown by molecular beam epitaxy, *Appl. Phys. Lett.* 73 (13) (1998) 1835–1837, <https://doi.org/10.1063/1.122298>.
- [17] R.E.L. Powell, S.V. Novikov, C.T. Foxon, A.V. Akimov, A.J. Kent, Photoluminescence of magnesium and silicon doped cubic GaN, *Phys. Status Solidi* 11 (3–4) (2014) 385–388, <https://doi.org/10.1002/pssc.201300468>.
- [18] H. Vilchis, V. Sánchez-R, Electrical behavior of Mg doped cubic GaN on c-GaN structure, *Mater. Sci. Semicond. Process.* 37 (2015) 68–72, <https://doi.org/10.1016/j.mssp.2015.01.052>.
- [19] H. Wang, A.-B. Chen, Calculation of shallow donor levels in GaN, *J. Appl. Phys.* 87 (11) (2000) 7859–7863, <https://doi.org/10.1063/1.373467>.
- [20] F. Mireles, S.E. Ulloa, Acceptor binding energies in GaN and AlN, *Phys. Rev. B* 58 (7) (1998) 3879–3887, <https://doi.org/10.1103/PhysRevB.58.3879>.
- [21] G. Kresse, J. Hafner, Ab initio molecular dynamics for liquid metals, *Phys. Rev. B* 47 (1) (1993) 558–561, <https://doi.org/10.1103/PhysRevB.47.558>, arXiv:0927-0256(96)00008.
- [22] C.G. Van de Walle, J. Neugebauer, First-principles calculations for defects and impurities: Applications to III-nitrides, *J. Appl. Phys.* 95 (8) (2004) 3851–3879, <https://doi.org/10.1063/1.1682673>.
- [23] C. Freysoldt, B. Grabowski, T. Hickel, J. Neugebauer, G. Kresse, A. Janotti, C. G. Van de Walle, First-principles calculations for point defects in solids, *Rev. Mod. Phys.* 86 (1) (2014) 253–305, <https://doi.org/10.1103/RevModPhys.86.253>.
- [24] A. Togo, I. Tanaka, First principles phonon calculations in materials science, *Scr. Mater.* 108 (2015) 1–5, <https://doi.org/10.1016/j.scriptamat.2015.07.021>.
- [25] X.H. Lu, P.Y. Yu, L.X. Zheng, S.J. Xu, M.H. Xie, S.Y. Tong, Evidence for a Type-II band alignment between cubic and hexagonal phases of GaN, *Appl. Phys. Lett.* 82 (7) (2003) 1033–1035, <https://doi.org/10.1063/1.1541113>.
- [26] J.L. Lyons, A. Janotti, C.G. Van de Walle, Carbon impurities and the yellow luminescence in GaN, *Appl. Phys. Lett.* 97 (15) (2010), 152108, <https://doi.org/10.1063/1.3492841>.
- [27] R. Armitage, Q. Yang, E.R. Weber, Analysis of the carbon-related “blue” luminescence in GaN, *J. Appl. Phys.* 97 (7) (2005), 073524, <https://doi.org/10.1063/1.1856224>.